Electron. Mater. Lett., Vol. 13, No. 1 (2017), pp. 57-65
DOI: 10.1007/s13391-017-6316-1

Interfacial Band-Edge Engineered TiO_2 Protection Layer on Cu_2O Photocathodes for Efficient Water Reduction Reaction

Jaesuk Choi,[1] Jun Tae Song,[2,3] Ho Seong Jang,[4] Min-Jae Choi,[1] Dong Min Sim,[1] Soonmin Yim,[1] Hunhee Lim,[1] Yeon Sik Jung,[1,*] and Jihun Oh[2,3,*]

[1]Department of Materials Science and Engineering, Korea Advanced Institute of Science and Technology (KAIST), Daejeon 34141, Korea
[2]Graduate School of EEWS (Energy, Environment, Water and Sustainability), Korea Advanced Institute of Science and Technology (KAIST), Daejeon 34141, Korea
[3]KAIST Institute for NanoCentury, Korea Advanced Institute of Science and Technology (KAIST), Daejeon 34141, Korea
[4]Materials Architecturing Research Center, Korea Institute of Science and Technology (KIST), Seoul 02792, Korea

(received date: 30 September 2016 / accepted date: 30 September 2016 / published date: 10 January 2017)

Photoelectrochemical (PEC) water splitting has emerged as a potential pathway to produce sustainable and renewable chemical fuels. Here, we present a highly active Cu_2O/TiO_2 photocathode for H_2 production by enhancing the interfacial band-edge energetics of the TiO_2 layer, which is realized by controlling the fixed charge density of the TiO_2 protection layer. The band-edge engineered Cu_2O/TiO_2 (where TiO_2 was grown at 80 °C via atomic layer deposition) enhances the photocurrent density up to −2.04 mA/cm^2 at 0 V vs. RHE under 1 sun illumination, corresponding to about a 1,200% enhancement compared to the photocurrent density of the photocathode protected with TiO_2 grown at 150 °C. Moreover, band-edge engineering of the TiO_2 protection layer prevents electron accumulation at the TiO_2 layer and enhances both the Faraday efficiency and the stability for hydrogen production during the PEC water reduction reaction. This facile control over the TiO_2/electrolyte interface will also provide new insight for designing highly efficient and stable protection layers for various other photoelectrodes such as Si, InP, and GaAs.

Keywords: water splitting, interfacial band-edge engineering, TiO_2, Cu_2O

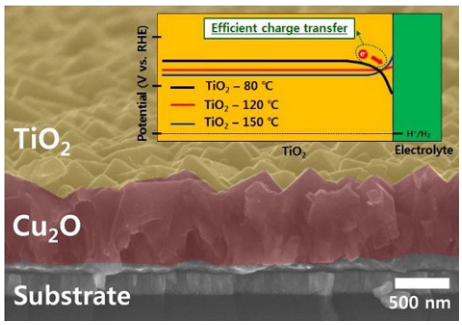

1. INTRODUCTION

Since the pioneering work on photoelectrochemical (PEC) water splitting by Fujishima and Honda,[1] enormous efforts have been dedicated to developing efficient, stable, and low-cost photoelectrodes to harvest solar energy in chemical fuels.[2,3] Metal oxides have advantages as photoelectrodes of being earth-abundant, non-toxic, and low-cost manufacturability. Within this context, cuprous oxide (Cu_2O), a *p*-type semiconductor with a favorable conduction band-edge position for the water reduction reaction, is considered one of the most promising candidates for an efficient and low-cost photocathode material for hydrogen production, due to its direct band-gap of 2.0 eV, the natural abundance of copper, and the possibility of large scale manufacturing.[4,5] However, Cu_2O typically undergoes reductive decomposition during the PEC water reduction reaction, and therefore prior research has mainly been focused on developing a protective layer on Cu_2O for a more stable and efficient PEC hydrogen evolution reaction.[6-11]

*Corresponding author: ysjung@kaist.ac.kr
*Corresponding author: jihun.oh@kaist.ac.kr

TiO_2 is known to have superior chemical durability in aqueous solutions with a wide range of pH, and thus has been explored for a robust protective layer on unstable photoelectrodes such as Cu_2O,[6-11] Si,[12-15] and GaAs[13] for PEC water reduction and oxidation reactions. In particular, Gratzel *et al.* demonstrated that TiO_2 coatings obtained by atomic layer deposition (ALD) produce a pin-hole free protective layer that stabilizes Cu_2O photocathodes up to 50 hours during the PEC hydrogen evolving reaction (HER).[8] When TiO_2 is used as a protective layer on Cu_2O, photo-generated electrons in Cu_2O traverse through the conduction band of TiO_2 and contribute to water reduction for hydrogen evolution at the TiO_2/electrolyte interface. Therefore, appropriate conduction band alignments of Cu_2O and TiO_2, relative to the water reduction redox potential, is crucial for more efficient charge injection to reduce water. For instance, Gratzel *et al*. inserted a thin aluminum doped ZnO (AZO) layer between Cu_2O and TiO_2 to facilitate charge transport from Cu_2O to TiO_2 by conduction band-edge alignment; the conduction band-edge position of Al-doped ZnO locates between those of Cu_2O and TiO_2.[10]

Alternatively, the band-edge position of a TiO_2 layer can be directly engineered to allow facile charge injection from the conduction band of Cu_2O by controlling the electrostatic field across the semiconductor interface without introducing additional interlayers. For instance, the electrostatic field across the semiconductor/electrolyte interface can be altered by introducing surface dipoles to shift the conduction band and valence band up or down in energy relative to the redox potential.[16,17] Organic dipole molecules have also been shown to perform well for this purpose in various types of solar devices; however, their use in solar water splitting devices is limited due to their poor stability under harsh conditions. In addition, selectively exposing crystal facets of the TiO_2 layer can also result in variation of the flat-band potential up to several hundred mV due to the facet-dependent surface charge distribution.[18-20] However, the inherent complexity of fabricating desired crystal facets significantly limits its application for a protective TiO_2 layer on unstable Cu_2O films. Thus, facile control of band-edges of the TiO_2 protection layer by controlling the electrostatic field is highly desired for efficient and durable hydrogen production by the PEC water splitting reaction but has not yet been addressed.

In this work, we present a practical strategy to manage interfacial band-edge energetics of a TiO_2 protective layer on Cu_2O films by controlling the fixed charge density of a TiO_2 layer formed by an ALD process. We identify that the deposition temperature of TiO_2 ALD plays a critical role in producing positive fixed charges in the TiO_2, which results in variation of the flat band potential of the TiO_2 layer of more than 300 mV. The conduction band-edge position of TiO_2 films grown at 80 °C (hereafter TiO_2 - 80 °C) is closer to the water reduction redox potential, and this results in a smaller energy barrier for the water reduction reaction than that obtained with TiO_2 grown at higher temperatures than 80 °C. Cu_2O films with TiO_2 - 80 °C (hereafter Cu_2O/TiO_2 - 80 °C) produce photocurrent density of about – 2.04 mA/cm^2 at 0 V (*vs*. RHE), a value that is about 12 times higher than that produced from Cu_2O films with TiO_2 grown at 150 °C (TiO_2 - 150 °C). In addition, facile electron transfer for the HER of Cu_2O/TiO_2 - 80 °C significantly improves the stability of the photocathode against corrosion over 12,000 s at 1 mA/cm^2 of photocurrent under simulated 1 sun illumination.

2. EXPERIMENTAL PROCEDURE

2.1 Fabrication of Cu_2O films

The Cu_2O films were synthesized by electrodeposition using a previously reported method.[21] The electrodeposition was conducted in a three-electrode system (WonATech, WBCS3000). The substrate for the electrodeposition was an ITO glass coated with Cu (~ 150 nm). Cu substrate was selected with reference to previous studies on Cu_2O. Thin films of Cu were deposited by electron beam evaporation with an adhesion layer of Cr with 15 nm. The electroplating bath was composed of 0.2 M $CuSO_4$ and 3 M lactic acid in 0.5 M K_2HPO_4 solution. The pH of the solution was adjusted to pH 12 by addition of a controlled amount of 2 M KOH solution. A Pt mesh (2.5 × 2.5 cm^2) and Ag/AgCl filled with a saturated KCl solution were used as a counter and reference electrode, respectively. The deposition temperature was maintained at 30 °C and Cu_2O electrodeposition was performed at 0.1 mA/cm^2 for 6000 seconds. The above chemicals were purchased from Sigma-Aldrich and used without further purification.

2.2 ALD of TiO_2 layer

The TiO_2 layers were deposited on Cu_2O/Cu/ITO and Si substrates using an ALD instrument (cn-1). Before the deposition, Cu_2O films were thoroughly washed with deionized (DI) water, and *p*-type Si (100) substrates were immersed for 30 s in a buffered oxide etch (BOE) solution to remove the native oxide, rinsed in deionized (DI) water, and dried with N_2 gas. Tetrakis-dimethyl-amido titanium (TDMAT, UP Chemical) and H_2O were used as a tinania precursor and a reactant. The deposition temperature was maintained at 80, 120 or 150 °C.

2.3 Pt catalyst deposition

Platinum catalysts were deposited using electron beam evaporation to improve the kinetics of the water reduction reaction. The thickness was 0.5 nm, estimated by a quartz crystal balance.

2.4 Thin film characterization

The cross-sectional images were observed using a field emission scanning electron microscope (FE-SEM, Hitachi S-4800). Spectroscopic ellipsometry (Alpha-se, J.A Woollam Co., Inc., USA) was used to characterize the thickness of TiO_2 films deposited on Si substrates. XRD and Grazing Incidence X-ray diffraction (GIXRD) data were obtained with a RIGAKU, D/MAX-2500. Total reflection spectra were measured on a UV-visible spectrometer (Shimadzu UV-3600) equipped with an integrating sphere (Shimadzu ISR-3100). Barium sulfate was used as a reference. X-ray photoelectron spectroscopy (XPS) data were collected with a multipurpose X-ray photoelectron spectrometer (Sigma Probe, Thermo VG Scientific). For C-V measurements, a Ni/Au (20/100 nm) metal contact on top of the TiO_2 layer was created by electron beam evaporation. The C-V measurements were performed at 100 kHz using a Keithley 4200-SCS semiconductor measurement system equipped with a Keithley 4225-PMU pulse generator, a 4225-RPM remote amplifier/switch, and a probe system.

2.5 Photoelectrochemical measurements

Photocurrent measurements were performed in 0.1 M KH_2PO_4 solution, using a three-electrode system. The electrolyte was purged with argon for at least 20 minutes before measurements. The reference electrode was Ag/AgCl in 3 M NaCl and a Pt wire served as a counter electrode. The illumination source was a 300 W Xe lamp and the intensity of incident light was calibrated with a Si diode to simulate AM1.5 illumination (100 mW/cm^2). The voltage-scan speed was 10 mV/s. Photocurrent stability tests were performed at 0 V versus RHE and 1 mA/cm^2. PEC measurement was conducted in dark and light conditions consecutively after sufficient Ar purging.

A Mott-Schottky analysis of TiO_2 grown at 80, 120, and 150 °C on ITO glass was conducted in the dark using a potentiostat/galvanostat (Biologic, SP-150). An ITO coated glass was used as a substrate for a Mott-Schottky analysis of TiO_2, as demonstrated in the literature.[10,13,16] The electrolyte is 1 M NaOH. The Mott-Schottky plots were obtained in a frequency range of 0.2-3 kHz with an amplitude of 10 mV. The potential was varied from 0.5 V *vs*. RHE to 1.75 V *vs*. RHE.

The electrochemical impedance spectroscopy (EIS) measurements for Cu_2O/TiO_2 - 80, 120, and 150 °C were performed using a Potentiostat/Galvanostat (Biologic, SP-150) in 0.1 M KH_2PO_4 solution. The frequencies were varied from 100 kHz to 1 Hz at 0 V *vs*. RHE. EIS experimental data were analyzed using EC-Lab software.

The Faradaic efficiency of the photocathodes was measured at 0 V *vs*. RHE during 2 hours in a single compartment cell. The reference electrode was Ag/AgCl in 3 M NaCl and a Pt wire served as a counter electrode. The electrolyte was 0.1 M KH_2PO_4 solution. The evolved gases after the PEC reaction were analyzed by gas chromatography (Inficon, Micro GC-3000). The Faradaic efficiency was calculated from the total amount of charge passed through the cell and the total amount of hydrogen generated. Note that Pt *vs*. Pt electrodes generated 93% of the Faradaic efficiency because a reverse reaction could occur in our single compartment cell.

3. RESULTS AND DISCUSSION

Figure 1a shows a tilted-view scanning electron microscope (SEM) image of a Cu_2O photocathode with a TiO_2 protective layer. Cu_2O films with thickness of 750 nm were electrodeposited on copper substrates and had a (111) preferred orientation (Fig. S1). A 45 nm-thick TiO_2 layer was deposited on the Cu_2O surface by ALD at 80, 120, and 150 °C. The TiO_2 deposition rate as a function of ALD cycles was 0.048-0.067 nm/cycles (Fig. S2). The TiO_2 thickness of 45 nm was determined to have minimum reflection of TiO_2/Cu_2O bilayers from the light reflectance

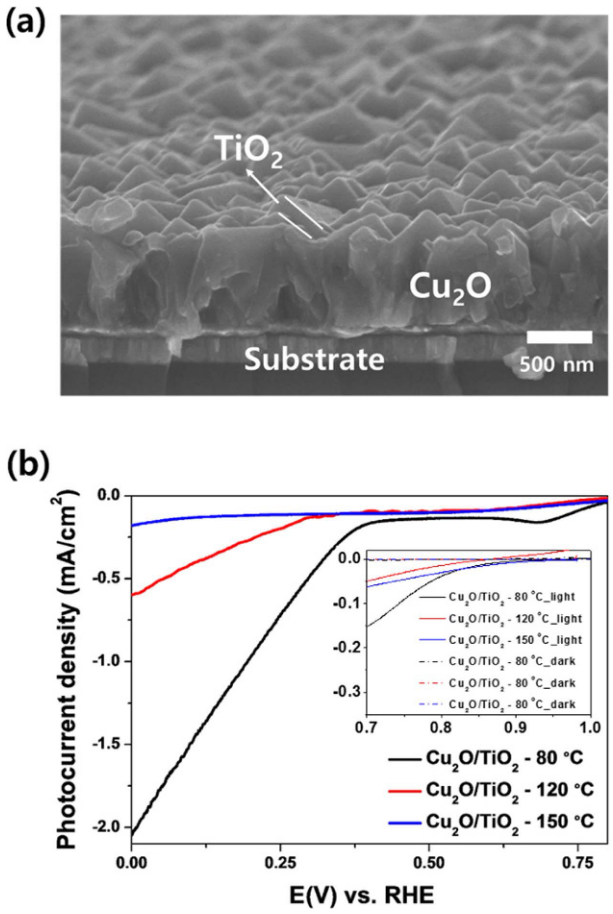

Fig. 1. (a) Cross-sectional views of Cu_2O films with TiO_2 - grown at 80 °C, and (b) current-potential curves of Cu_2O/TiO_2 - 80, 120, and 150 °C in the dark and under illumination.

measurement (80 °C sample). 45 nm-thick TiO_2 on the Cu_2O bilayer shows the most effectively suppressed light reflectance in the visible light range among the samples (Fig. S3). It is confirmed that TiO_2 films prepared by the ALD process at these deposition temperatures exhibit highly conformal coverage on the Cu_2O surface (Fig. 1a and S4). An X-ray diffraction (XRD) analysis was performed to investigate the properties of TiO_2 layers grown at 80, 120, and 150 °C on a glass substrate. Figure S5a shows that the TiO_2 is amorphous. Grazing-incidence XRD (GIXRD) also confirmed that the TiO_2 - 150 °C is amorphous (Fig. S5b). Also, our ALD TiO_2 layer is sub-stoichiometric with reduced Ti^{3+} species on the surface, which is a typical feature of ALD-deposited TiO_2 using a TDMAT precursor (Fig. S6). The reduced Ti^{3+} species can be removed if titanium isopropoxide is used as a precursor in the ALD process.

Figure 1b shows the PEC current-potential (*J-V*) curves of the Cu_2O/TiO_2 - 80, 120, and 150 °C for HER under simulated 1 sun illumination. All Cu_2O/TiO_2 - x °C electrodes had Pt catalysts (approximately 0.5 nm) on the surface to improve the kinetics of the water reduction reaction. As shown in Fig. 1b, the photocurrent density dramatically improves with decreasing deposition temperature of TiO_2. For instance, the photocurrent density increases from 0.17 to 2.04 mA/cm^2 at 0 V (*vs.* RHE) when the deposition temperature of TiO_2 is decreased from 150 to 80 °C. In the magnified plot (inset of Fig. 1b), the TiO_2 deposited at 80 °C shows distinct photocurrent for HER. The onset potential, which is defined as the potential allowing photocurrent over 0.1 mA/cm^2, is also different depending on the temperature. The Cu_2O/TiO_2 - 80 °C exhibits 200-300 mV shifted onset potential, 0.74 V, as compared to Cu_2O films with TiO_2 formed at higher temperature (0.52 V for 120 °C and 0.42 V for 150 °C). This indicates that electrons at Cu_2O/TiO_2 - 80 °C can be more easily transferred for the HER at lower applied potential as compared to other samples. We note that the small peak at around 0.69 V for only the 80 °C sample is believed to originate, in part, from the larger amount of H_2 gas adsorption than others.[6] In order to exclude possible thermal annealing effects on the PEC property of Cu_2O during ALD TiO_2 deposition at high temperature, we simply placed Cu_2O in the ALD chamber at 150 °C without introducing TiO_2 precursors for the duration of the TiO_2 deposition time, and compared the PEC *J-V* curves of Cu_2O with and without annealing in the ALD chamber (see Fig. S7). Figure S7 shows that heating Cu_2O at 150 °C in the ALD chamber results in a nearly identical PEC response to that of Cu_2O without annealing. It should be noted that a significant portion of the photocurrent density at positive potential would come from the reductive decomposition of Cu_2O.[9] This suggests that the TiO_2 layers deposited at different temperatures are crucial to determine the PEC behavior of Cu_2O/TiO_2 photocathodes. Since it is

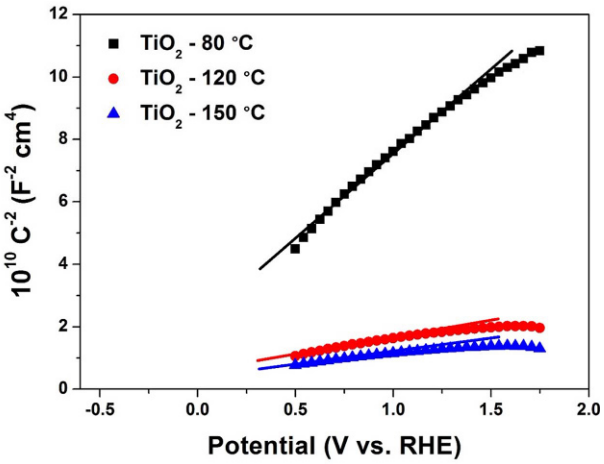

Fig. 2. Mott-Schottky plots for TiO_2 grown at 80, 120, and 150 °C on ITO glass.

well known that the PEC response is affected by the electrical conductivity and the band-edge position of a photocathode, the electrical properties of TiO_2 and band-edge energetics at the TiO_2/electrolyte interface should be heavily dependent on the ALD TiO_2 deposition temperature.

A Mott-Schottky analysis was employed on ALD TiO_2 films grown at 80, 120, and 150 °C on ITO glass to determine the donor density and flat-band potential, as shown in Fig. 2. Figure 2 shows representative Mott-Schottky plots obtained at a frequency of 940.3 Hz. Note that Mott-Schottky plots in other frequency ranges are almost the same (see Fig. S8). The donor density (N_D) and flat-band potential (E_{fb}) were calculated from the slopes and x-intercept given by Equation (1), which expresses the relation of the depletion layer capacitance (C) at the surface of the TiO_2 electrode and the applied potential (E), respectively.

$$\frac{A^2}{C^2} = \frac{2}{e\varepsilon\varepsilon_0 N_D}\left(E - E_{fb} - \frac{kT}{e}\right) \quad (1)$$

In Equation (1), A is the electrode area, the dielectric constant (ε) of TiO_2 is 75,[22] ε_0 is the permittivity of the vacuum, k is the Boltzmann constant, e is the electronic charge (1.6×10^{19} C), and T is 298 K. The difference between the conduction band position (E_{CB}) and the Fermi energy level (E_F) is determined as follows

$$E_{CB} - E_F = \frac{kT}{e}\ln\frac{N_C}{N_D} \quad (2)$$

where the effective density of states in the conduction band N_C for TiO_2 is 7.8×10^{20} cm^{-3}.[10] Table 1 summarizes the calculated values of N_D, E_{FB}, and E_{CB}-E_F. For instance, the N_D values of TiO_2 - 80, 120, and 150 °C are 3.23×10^{19}, 1.76×10^{20}, and 2.66×10^{20} cm^{-3}, respectively. The calculated dopant density of our ALD TiO_2 is higher than ALD TiO_2

Table 1. Electrical properties of the TiO_2 layer grown at x °C, obtained from Mott-Schottky analysis.

Layer	E_{fb} (V/RHE)	N_D (cm^{-3})	$E_{CB} - E_F$ (mV)
TiO_2 - 80 °C	−0.343 ± 0.02	(3.22 ± 0.04) × 10^{19}	81.9 ± 0.3
TiO_2 - 120 °C	−0.581 ± 0.03	(1.77 ± 0.03) × 10^{20}	38.1 ± 0.38
TiO_2 - 150 °C	−0.672 ± 0.03	(2.65 ± 0.05) × 10^{20}	27.7 ± 49

deposited with H_2O_2 as an oxygen source.[15,16] It is well known that the carrier density of ALD TiO_2 is dependent on the oxygen source, which influences oxygen vacancies in TiO_2; ALD TiO_2 by H_2O as oxygen source (used in this work) results in a higher carrier concentration than TiO_2 obtained with H_2O_2, which provides fewer oxygen vacancies. The dopant density of TiO_2 deposited at higher temperature is higher than that of TiO_2 at lower temperature. However, TiO_2 - 80 °C has the highest photocurrent density in Fig. 1b, although the doping density is the lowest. Although higher dopant density generally increases the conductivity of a material, the electron transport through the conduction band of TiO_2 with few tens of nanometer thickness was shown to have negligible ohmic loss even with comparatively low dopant density (10^{17} cm^{-3}).[12] Since all of the prepared TiO_2 layers have dopant densities greater than 10^{19} cm^{-3} and the thickness is only 45 nm, it is expected that the photo-generated electrons can traverse through the conduction band of the TiO_2 layer with negligible ohmic loss. Therefore, the difference of conductivity is not responsible for the enhanced PEC J-V characteristics of Cu_2O/TiO_2 - 80 °C.

As listed in Table 1, however, the TiO_2 deposited at higher temperature has a more negative flat-band potential with respect to the HER redox level. For instance, the E_{FB} values of TiO_2 - 80, 120, and 150 °C are −0.343, −0.581, and −0.672 V *vs.* RHE, respectively. According to the Gerischer model, electron transfer occurs from the occupied state in the conduction band of a semiconductor to an empty state in the redox system; larger overlap between the conduction band-edge and the redox potential would generate higher electron transfer.[23] Therefore, TiO_2 with a slightly higher conduction band edge position (i.e, more negative on the electrochemical energy scale) than the HER redox potential would facilitate more electron transfer for the HER and produce higher photocurrent density for the HER. If the conduction band-edge position of TiO_2 is too negative with respect to the HER redox potential, the overlap between the conduction band and the redox potential would decrease and the charge transfer would be impeded. Since the flat-band potentials of TiO_2 at 80 °C and 150 °C are −0.343 V and −0.672 V, respectively, it is anticipated that the ALD TiO_2 layers deposited at 80 °C would produce higher photocurrent.

Figure 3 depicts band diagrams of TiO_2 deposited at various temperatures on Cu_2O photocathodes in dark and under illumination during the HER, based on the optoelectric and conduction band-edge positions of TiO_2 obtained from the Mott-Schottky plot and band-gap from a Tauc plot (Fig. S9). The band diagrams for the Cu_2O/TiO_2 photocathode with TiO_2 grown at 80, 120, and 150 °C biased at 0 V *vs.* RHE in the dark are shown in Fig. 3a, constructed with data for Cu_2O from the literature.[10] Since all TiO_2 layers have high dopant densities of more than 10^{19} cm^{-3}, the Cu_2O/TiO_2 heterojunctions show almost the same behavior regardless of the ALD deposition temperature. Therefore, the energy band alignment at the TiO_2/electrolyte interfaces was explored to explain the observed PEC responses of Cu_2O/TiO_2 - 80, 120, and 150 °C in more detail. Figure 3b displays the band

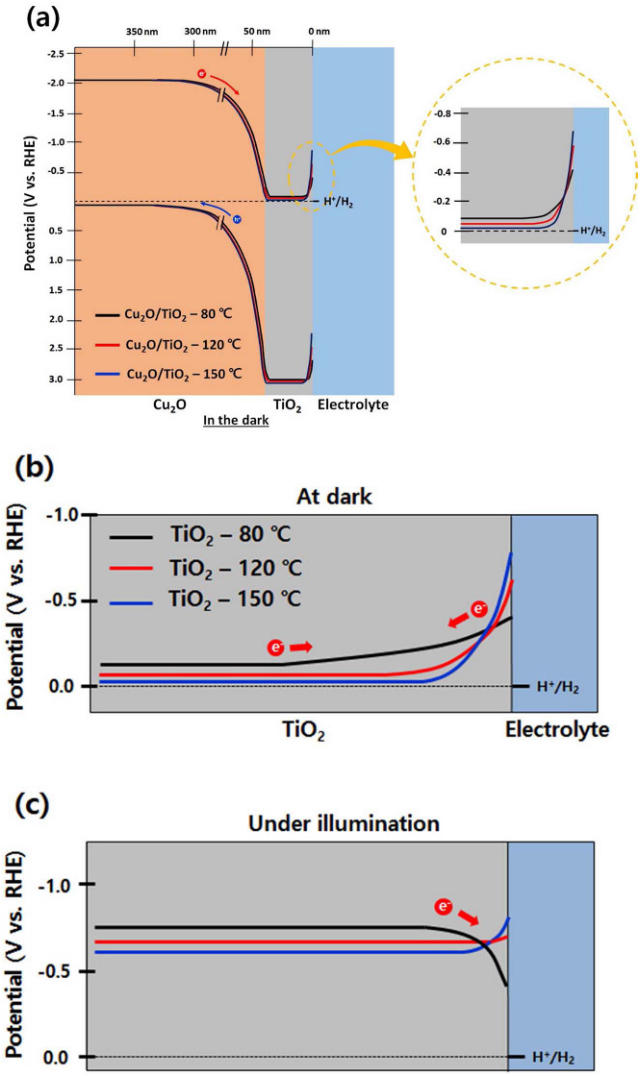

Fig. 3. (a) Band diagram for Cu_2O/TiO_2 photocathode with TiO_2 grown at 80, 120, and 150 °C biased at 0 V vs. RHE in the dark. Schematic band diagrams of Cu_2O/TiO_2 - 80, 120, and 150 °C near the surface (b) in the dark and (c) under illumination at 0 V vs. RHE.

diagrams of the photocathodes in the dark at 0 V *vs*. RHE. From the illustration, it could be seen that large energy barriers at the TiO_2/electrolyte interface form for all samples, and this prevents charge transfer and generates negligible dark currents. Although there is some probability of electron tunneling through thin energy barriers, the low photocurrent density of TiO_2 - 120 and 150 °C at highly negative applied potentials, as shown in Fig. S10, indicates that the photocurrent induced by electron tunneling might be negligible with respect to the PEC performance of our photocathodes. Figure 3c shows the band diagrams of these Cu_2O/TiO_2 photocathodes under illumination: the photovoltage generated in Cu_2O, i.e., 0.6 V,[8] was added to allow the potentials to be reductive in the band diagrams under illumination. As shown in Fig. 3c, the energy barrier disappears as the conduction band-edges of Cu_2O/TiO_2 - 80 °C indeed move into the accumulation mode at 0 V *vs*. RHE. In contrast, the electrons in Cu_2O/TiO_2 - 120 and 150 °C do not have enough energy to surmount this barrier, consequently producing low photocurrent at this potential. Since the flat-band potential of TiO_2 - 120 °C is about 91 mV higher than that of TiO_2 - 150 °C, the energy barrier of TiO_2 - 120 °C disappears at lower applied potential than TiO_2 - 150 °C. Therefore, TiO_2 - 120 °C generates a higher photocurrent than TiO_2 - 150 °C, and the onset voltage was larger for higher TiO_2 deposition temperature, as shown in

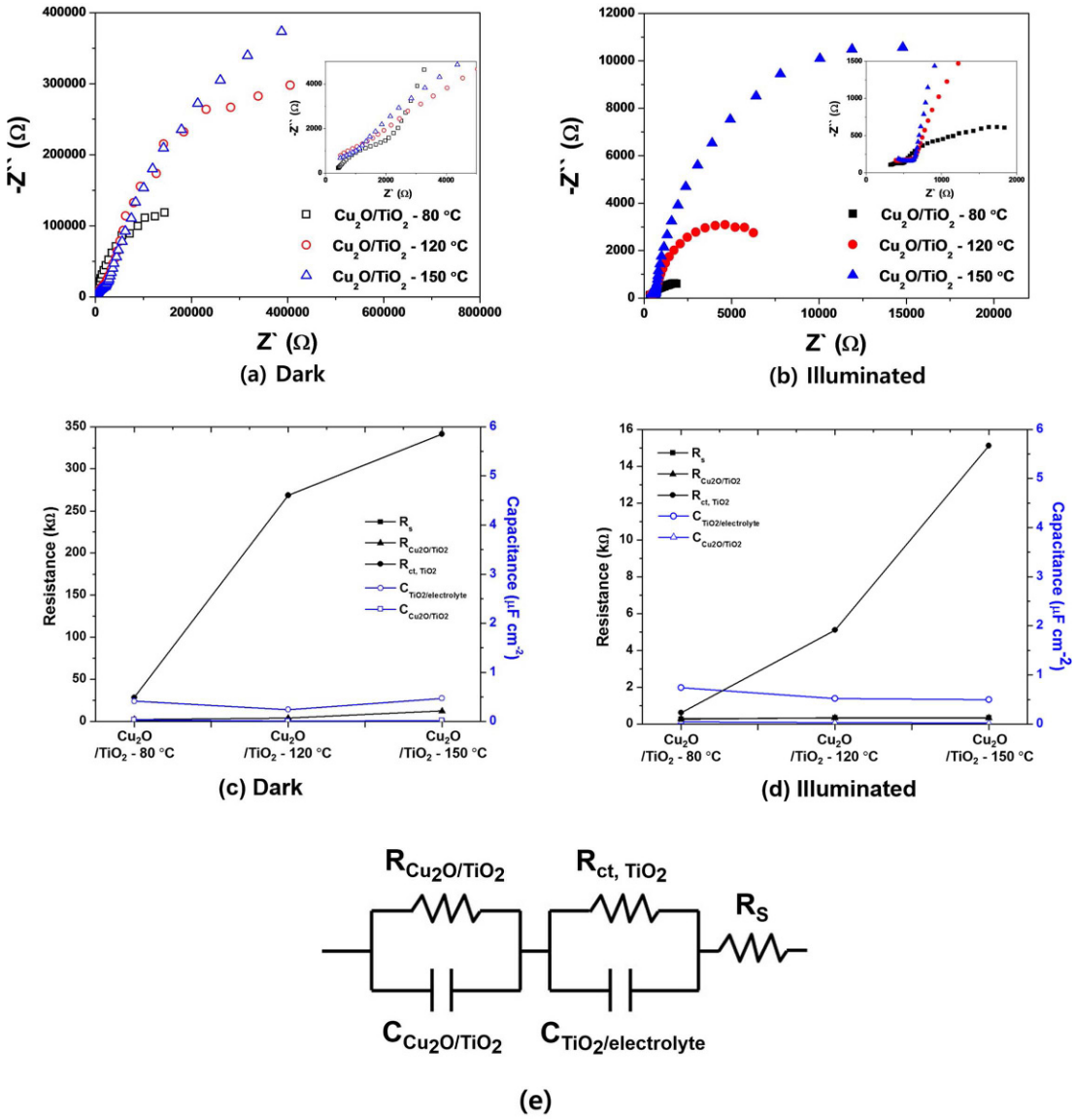

Fig. 4. Nyquist plots measured for $Cu_2O/TisO_2$ - 80, 120, and 150 °C, (a) in the dark and (b) under illumination at 0 V vs. RHE. Representation of charge transfer resistance and capacitance values (c) in the dark, and (d) under illumination for the equivalent circuit in (e). (e) Electronic equivalent circuit representing the Cu_2O/TiO_2/electrolyte used for EIS data modeling.

Fig. 3. Hence, the ALD TiO_2 deposition temperature directly affects the TiO_2/electrolyte energetics, and is responsible for the PEC response of Cu_2O/TiO_2 photocathodes.

Electrochemical impedance spectroscopy (EIS) was carried out at 0 V *vs.* RHE in the dark and under illumination to study the kinetics of interfacial charge transfer in the multiple junctions of Cu_2O/TiO_2. Figures 4a and 4b show the Nyquist plots of Cu_2O/TiO_2 photocathodes in dark and under illumination, respectively. As shown in Figs. 4a and b, the smaller arcs for the electrodes under illumination indicate increased conductivity of the photoelectrodes by illumination. Figures 4c and d show the fitted data of Nyquist plots for all Cu_2O/TiO_2 samples with the equivalent circuit model expressed in Fig. 4e. The fitted resistances and capacitances with fitting errors are summarized in Table S1. The equivalent circuit consists of the interface resistance between Cu_2O and TiO_2, $R_{Cu2O/TiO2}$, the charge transfer resistance from the conduction band of the TiO_2 to electrolyte side, $R_{ct,TiO2}$, the series resistance, R_s, the capacitance of the Cu_2O/TiO_2 heterojuctions, $C_{Cu2O/TiO2}$, and the capacitance of surface junctions, $C_{TiO2/electrolyte}$. Importantly, the $R_{ct,\ TiO2}$, which corresponds to the semicircles at higher frequencies in the Nyquist plots, increases with the deposition temperature of TiO_2 with and without illumination. This reflects more efficient charge transfer across the TiO_2/electrolyte interfaces for TiO_2 samples deposited at lower temperature. The values of R_S, $R_{Cu2O/TiO2}$, $C_{TiO2/electrolyte}$, and $C_{Cu2O/TiO2}$ are independent of the deposition temperature of TiO_2 by ALD, and this trend is consistent with the observed Nyquist plots and the band diagrams depicted in Fig. 3. However, it is obvious that the charge transfer resistance, $R_{ct,\ TiO2}$, is considerably reduced with a decrease in the deposition temperature, implying that a smaller difference between the flat-band potential of the TiO_2 layer and the HER level generates smaller resistance to charge transfer across the TiO_2/electrolyte interfaces. By characterizing the electrodes with Mott-Schottky plots, band diagrams models, and an EIS analysis, the roles of the flat-band potentials presented in TiO_2 layers with different deposition temperatures are elucidated. The results indicate that the band alignment of the TiO_2 layer at the TiO_2/electrolyte interface as a function of the deposition temperature is responsible for the improvement of the photocurrent density of the Cu_2O/TiO_2 photoelectrode obtained with lower TiO_2 deposition temperature.

It is well known that the negative or positive fixed charges in a film at the semiconductor/electrolyte junction can alter the position of the energy bands, shifting the conduction band and valence band up or down in the electron energy scale, compared to the film without fixed charges. In order to elucidate the fixed charge density in the TiO_2 layer as a function of the deposition temperature, we performed capacitance-voltage (C-V) characterization with metal-oxide-semiconductor (MOS) structures. Figure S11 shows

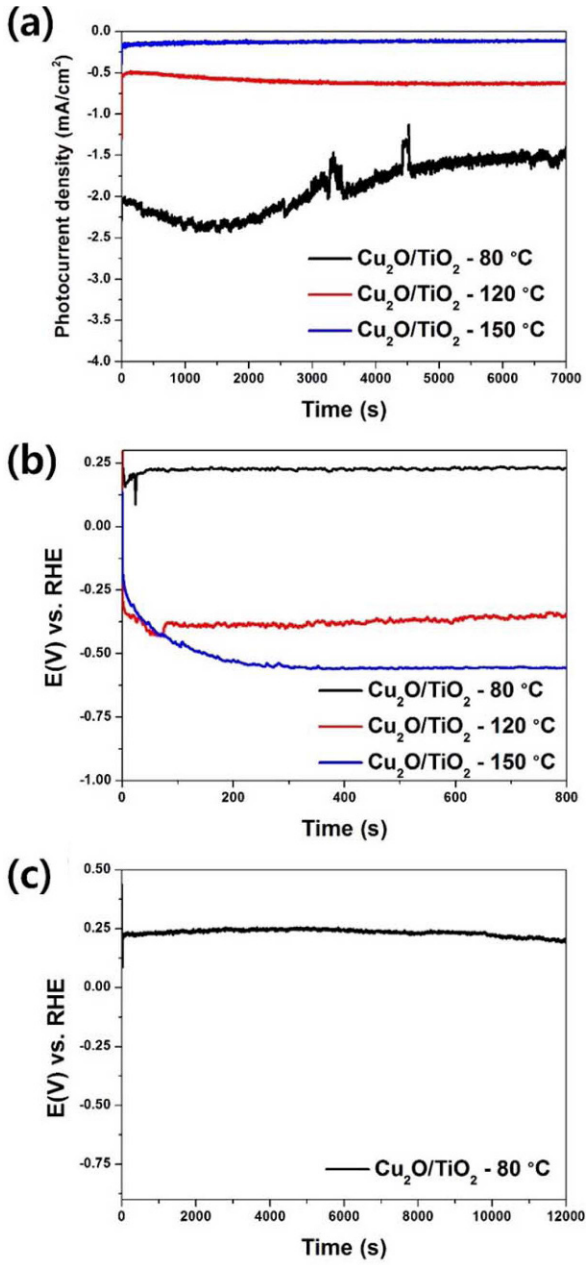

Fig. 5. (a) Chronoamperometric measurements at 0 V vs. RHE for Cu_2O/TiO_2 - 80, 120, and 150 °C. (b) Electrochemical potential required to maintain 1mA/cm^2 for Cu_2O/TiO_2 - 80, 120, and 150 °C. (c) Cu_2O/TiO_2 - 80 °C exhibited good stability over 12000 s.

the C-V characteristics of TiO_2 on Si MOS capacitors, indicating that the measured flat-band voltage values of metal/TiO_2 - 80, 120, 150 °C /Si are −1.66, −1.50, and −1.39 V, respectively. Since the flat-band voltage in a MOS capacitor shifts to more negative voltages as the positive fixed charge density in the film increases, positive fixed charge is contained in ALD TiO_2 films and the positive fixed charge density in a TiO_2 film increases with decreasing

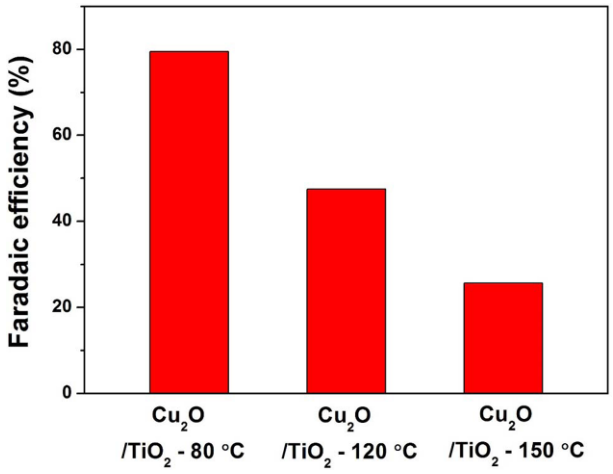

Fig. 6. Real hydrogen production using Cu_2O/TiO_2 - 80, 120, and 150 °C at 0 V vs. RHE after 2 hours. For reference, Pt vs. Pt electrodes generated 93 % of Faradaic efficiency.

deposition temperature of ALD TiO_2. It should be noted that the incorporation of negative fixed charges in TiO_2 films can cause the same flat-band voltage shift but in this case fewer negative fixed charges in the TiO_2 films would shift the flat-band voltage negatively, although increasing positive fixed charge density in a dielectric film with decreasing deposition temperature in chemical vapor deposition processes was reported. Therefore, modification of the amount of fixed charge density in the TiO_2 film by controlling the ALD deposition temperature alters the flat-band potentials and appropriate band-edge alignment at the TiO_2-water interface at lower deposition temperature. Our TiO_2 - 80 °C on Cu_2O produces roughly −2.04 mA/cm^2 photocurrent density at a potential of 0 V vs. RHE even without using an interfacial AZO layer. Note that the photocurrent density of a Cu_2O/AZO/TiO_2 photocathode at 0 V vs. RHE is about −5.0 mA/cm^2 in mild pH conditions.[8] Note also that TiO_2 films deposited at various temperatures have the same surface stoichiometry, as seen in the X-ray photoelectron spectroscopy (XPS) data (Fig. S6).

Figure 5 shows stability tests of Cu_2O/TiO_2 - 80, 120, and 150 °C photocathodes at 0 V *vs*. RHE under illumination. As shown in Fig. 5a, constant photocurrent density regardless of the deposition temperature TiO_2 by ALD was observed for 2 hours, indicating that all TiO_2 layers stabilize the Cu_2O through reductive decomposition during PEC HER. Note that the fluctuation in the photocurrent originates from the formation and detachment of hydrogen bubbles on the photocathodes. Additionally, chronopotentiometry tests were carried out to examine the stability of the photocathodes under 1 mA/cm^2 under illumination. As shown in Fig. 5b, Cu_2O with TiO_2 - 120 and 150 °C show a rapid increase of the HER overpotential within 1 minute and severe degradation was visible to the naked eye in a short time. In contrast, Cu_2O with TiO_2 - 80 °C exhibits excellent stability, maintaining a constant potential at 1 mA/cm^2 for 12000 seconds, as shown in Fig. 5c. This demonstrates that the TiO_2 - 80 °C layer employed in our studies not only improves the PEC response but also stabilizes the buried Cu_2O films efficiently.

Figure 6 shows the HER Faradaic efficiencies of the Cu_2O/TiO_2 photocathodes after 2 hours of the stability test at 0 V *vs.* RHE measured by gas chromatography. As shown in Fig. 6, the HER Faradaic efficiency for Cu_2O/TiO_2 - 80, 120, and 150 °C are 79.5, 47.5, and 25.6%, respectively. It should be noted that the Faradaic efficiency is measured using a single compartment cell, which might underestimate the hydrogen production Faradaic reaction due to the hydrogen reduction reaction at the counter electrode. It is surprising that even though all Cu_2O/TiO_2 samples exhibit constant photocurrent densities in Fig. 5a, the Cu_2O/TiO_2 - 120 and 150 °C samples show Faradaic efficiency less than 50%. This indicates that other reactions occurred simultaneously in TiO_2 deposited at higher temperatures. As revealed by XPS data in Fig. S12, after the tests, the shoulders around 459 eV, denoting the formation of Ti^{3+}, increase in Cu_2O/TiO_2 - 120 and 150 °C. This indicates that when an unfavorable conduction band-edge for electron injection in TiO_2 layer exists, the photoelectrons from Cu_2O accumulate and accelerate the formation of Ti^{3+} in TiO_2 rather than inject across the TiO_2/electrolyte interfaces to reduce water. Also, no Cu peak is shown after the stability test, indicating that no Cu_2O corrosion reaction occurs in this examination (Fig. S13). Therefore, energetically favorable band alignment near the surface is crucial for producing hydrogen at 0 V *vs.* RHE efficiently.

4. CONCLUSIONS

In summary, we introduced a facile and effective methodology to engineer the interfacial band-edge energetics of the TiO_2 layer for water reduction by controlling the deposition temperature of TiO_2 by ALD. The band-edge position of the ALD TiO_2 layers was controlled by modifying the fixed charge density in the TiO_2 layer by controlling the deposition temperature: the low temperature TiO_2 provides efficient charge transfer across the surface due to energetically favorable conduction band-edges. As a result, a photocurrent density of −2.04 mA/cm^2 at 0 V *vs.* RHE with stability for more than 2 hours during PEC HER was obtained for the Cu_2O protected with 80°C-deposited TiO_2. Moreover, the smaller energy barrier for electron injection at the TiO_2/water interface of the TiO_2 layer grown at 80 °C also provides significantly higher hydrogen Faraday efficiency by preventing electron accumulation at the TiO_2/water interface and reduction of TiO_2. Because the

energetically favorable band alignment near the surface is a primary factor for overall efficient and stable PEC responses, our approach will be beneficial for designing more stable and efficient protective layers that are widely effective for various unstable photocathodes.

ACKNOWLEDGEMENTS

This work was supported by the Korea Institute of Energy Technology Evaluation and Planning(KETEP) and the Ministry of Trade, Industry & Energy(MOTIE) of the Republic of Korea (No. 20132020000270). This work was also supported by the Korea CCS R&D Center (KCRC) grant funded by the Korea government (Ministry of Education, Science and Technology) (No. NRF-2014M1A8A1049303).

Electronic Supplemental Materials: The online version of this article (DOI: 10.1007/s13391-017-6316-1) contains supplemental materials.

REFERENCES

1. A. Fujishima and K. Honda, *Nature* **238**, 37 (1972).
2. M. G. Walter, E. L. Warren, J. R. McKone, S. W. Boettcher, Q. X. Mi, E. A. Santori, and N. S. Lewis, *Chem. Rev.* **110**, 6446 (2010).
3. Z. S. Li, W. J. Luo, M. L. Zhang, J. Y. Feng, and Z. G. Zou, *Energy Environ. Sci.* **6**, 347 (2013).
4. W. Wang, W. Zhang, S. Meng, L. Jia, M. Tan, C. Hao, Y. Liang, J. Wang, and B. Zou, *Electron. Mater. Lett.* **12**, 753 (2016).
5. H. Kim, S.-H. Kim, K. Y. Ko, H. Kim, J. Kim, J. Oh, and H.-B.-R. Lee, *Electron. Mater. Lett*. **12**, 404 (2016).
6. P. C. Dai, W. Li, J. Xie, Y. M. He, J. Thorne, G. McMahon, J. H. Zhan, and D. W. Wang, *Angew. Chem. Int. Ed.* **53**, 13493 (2014).
7. C. L. Li, T. Hisatomi, O. Watanabe, M. Nakabayashi, N. Shibata, K. Domen, and J. J. Delaunay, *Energy Environ. Sci.* **8**, 1493 (2015).
8. S. D. Tilley, M. Schreier, J. Azevedo, M. Stefik, and M. Graetzel, *Adv. Funct. Mater.* **24**, 303 (2014).
9. A. Paracchino, V. Laporte, K. Sivula, M. Gratzel, and E. Thimsen, *Nat. Mater.* **10**, 456 (2011).
10. A. Paracchino, N. Mathews, T. Hisatomi, M. Stefik, S. D. Tilley, and M. Gratzel, *Energy Environ. Sci.* **5**, 8673 (2012).
11. C. G. Morales-Guio, S. D. Tilley, H. Vrubel, M. Gratzel, and X. L. Hu, *Nat. Commun.* **5** (2014).
12. B. Seger, T. Pedersen, A. B. Laursen, P. C. K. Vesborg, O. Hansen, and I. Chorkendorff, *J. Am. Chem. Soc.* **135**, 1057 (2013).
13. S. Hu, M. R. Shaner, J. A. Beardslee, M. Lichterman, B. S. Brunschwig, and N. S. Lewis, *Science* **344**, 1005 (2014).
14. B. Seger, D. S. Tilley, T. Pedersen, P. C. K. Vesborg, O. Hansen, M. Gratzel, and I. Chorkendorff, *RSC Adv.* **3**, 25902 (2013).
15. B. Seger, S. D. Tilley, T. Pedersen, P. C. K. Vesborg, O. Hansen, M. Gratzel, and I. Chorkendorff, *J. Mater. Chem. A* **1**, 15089 (2013).
16. G. Ashkenasy, D. Cahen, R. Cohen, A. Shanzer, and A. Vilan, *Accounts Chem. Res.* **35**, 121 (2002).
17. S. Ruhle, M. Greenshtein, S. G. Chen, A. Merson, H. Pizem, C. S. Sukenik, D. Cahen, and A. Zaban, *J. Phys. Chem. B* **109**, 18907 (2005).
18. R. Hengerer, L. Kavan, P. Krtil, and M. Gratzel, *J. Electrochem. Soc.* **147**, 1467 (2000).
19. C. W. Kim, S. J. Yeob, H.-M. Cheng, and Y. S. Kang, *Energy Environ. Sci.* **8**, 3636 (2015).
20. Y. F. Lu, D. J. Choi, J. Nelson, O. B. Yang, and B. A. Parkinson, *J. Electrochem. Soc.* **153**, E131 (2006).
21. A. Paracchino, J. C. Brauer, J. E. Moser, E. Thimsen, and M. Graetzel, *J. Phys. Chem. C* **116**, 7341 (2012).
22. D. M. King, X. H. Du, A. S. Cavanagh, and A. Weimer, *Nanotechnology* **19**, 445401 (2008).
23. H. Gerische, *J. Chim. Phys. Pcb* **70**, 584 (1973).